NIH Public Access
Author Manuscript
Magn Reson Med. Author manuscript; available in PMC 2013 September 01.

Published in final edited form as:
Magn Reson Med. 2012 September ; 68(3): 822–829. doi:10.1002/mrm.23305.

Free-Breathing Inner-Volume Black-Blood Imaging of the Human Heart Using Two-dimensionally Selective Local Excitation at 3T

Khaled Z. Abd-Elmoniem[1], **Christoph Barmet**[4], and **Matthias Stuber**[2,3,5]

[1]Biomedical and Metabolic Imaging Branch, National Institute of Diabetes and Digestive and Kidney Diseases, National Institutes of Health, Bethesda, MD, USA [2]The Department of Medicine, Cardiology Division, Johns Hopkins University School of Medicine, Baltimore, MD, USA [3]The Department of Electrical and Computer Engineering, Johns Hopkins University, Baltimore, MD [4]Institute for Biomedical Engineering, University and ETH Zurich, Switzerland [5]Department of Radiology, University Hospital Lausanne, and Center for Biomedical Imaging (CIBM), Lausanne, Switzerland

Abstract

Black-blood fast spin-echo imaging is a powerful technique for the evaluation of cardiac anatomy. To avoid fold-over artifacts, using a sufficiently large field of view in phase-encoding direction is mandatory. The related oversampling affects scanning time and respiratory chest motion artifacts are commonly observed. The excitation of a volume that exclusively includes the heart without its surrounding structures may help to improve scan efficiency and minimize motion artifacts. Therefore, and by building on previously reported inner-volume approach, the combination of a black-blood FSE sequence with a two-dimensionally selective radiofrequency pulse is proposed for selective “local excitation” small-FOV imaging of the heart. This local excitation technique has been developed, implemented, and tested in phantoms and *in vivo*. With this method, small-FOV imaging of a user-specified region in the human thorax is feasible, scanning becomes more time efficient, motion artifacts can be minimized and additional flexibility in the choice of imaging parameters can be exploited.

Keywords

2D-selective RF Pulses; Black-Blood; local excitation

INTRODUCTION

Black-blood-prepared (BB) fast spin-echo (FSE) magnetic resonance imaging (MRI) is a valuable tool for non-invasive imaging of the cardiovascular anatomy (1,2). To avoid fold-over artifacts, a sufficiently large field of view (FOV) in fold-over direction is often mandatory but inevitably comes at the expense of scanning time. Nevertheless, and since such a large FOV does not only include the anatomy of interest, respiratory motion artifacts originating from the moving chest wall often have a detrimental impact on image quality. Constraining the FOV in fold-over direction using pre-pulses or saturation slabs (1–3) may require additional pre-pulses and gradient refocusing and the quality of the suppression outside of the desired FOV remains T1-dependent. In addition, the prolonged echo time

Corresponding Author: Khaled Z. Abd-Elmoniem, Ph.D., Biomedical and Metabolic Imaging Branch, National Institute of Diabetes and Digestive and Kidney Diseases, National Institutes of Health, Building 10, CRC Room 3-5340, Bethesda, MD 20892, Tel: (301) 451-434, abdelmoniemkz@mail.nih.gov.

$watermark-text
$watermark-text
$watermark-text

$watermark-text

$watermark-text

$watermark-text

(TE) associated with some of these techniques inevitably leads to more pronounced T2*-related artifacts, lower signal-to-noise (SNR) ratio, and reduced overall image quality, which may be further amplified at high magnetic field strength (4,5).

Inner-volume excitation (6) and multidimensional spatially-selective RF were introduced more than two decades ago (6–9). The use of 2D-selective pulses for local excitation as part of a spin echo experiment was also described by Pauly et al. (10). Since then, a steadily growing number of applications for 2D-selective pulses have been reported, facilitated by advances in gradient hardware and the demand for fast imaging. Recently, the use of self-refocused 2D-selective RF pulses that account for T2*-dependent relaxation during the excitation has been reported for sharper FOV localization and better outer-volume suppression (2,11–16). While the theoretical aspects of these strategies show a potential for removing the need for refocusing gradients, and thereby shortening the minimum TE, practical implementations have only been demonstrated in phantoms (11,15), at low field strength (1,14,17), and for imaging stationary or slow-moving organs (1–3,13,14,17,18). However, detailed investigation of 2D spatially selective excitation for small-FOV inner-volume free-breathing cardiac imaging has not been exploited to our knowledge.

The objective of this work was therefore to develop and examine the utility of 2D local excitation (LocEx) as part of the inner-volume imaging technique for small-FOV *in vivo* black-blood cardiovascular MRI at 3T to test the hypotheses that 1) time efficiency can be improved with LocEx, 2) motion artifacts can be reduced, and 3) additional flexibility in the choice of imaging parameters can be exploited when compared to more conventional non-local excitation techniques. The local excitation method was implemented for black-blood cardiac imaging as part of a free-breathing navigator gated and corrected dual-inversion FSE imaging sequence at high magnetic field strength. For local excitation, the initial 90° RF pulse of the FSE sequence was replaced by a user-specified 2D-selective cylindrical excitation and followed by a series of orthogonal slice selective refocusing pulses to obtain exclusive signal from a “disc” with user-specified diameter and slice thickness.

METHODS

Background

A typical electrocardiogram (ECG) triggered free-breathing black-blood (BB) FSE sequence as shown in Figure 1 consists of a dual inversion (DIR) pre-pulse followed by an inversion delay (TI), the navigator for motion artifact suppression, and the FSE signal-readout (19,20). Typically, the FSE module incorporates a non-selective or slice-selective 90° pulse followed by a train of slice-selective 180° refocusing pulses. To maximize the contrast between the blood and the myocardium, the image is commonly acquired when signal-nulling of the in-flowing blood-pool magnetization occurs (21) at $TI=-T_1\ln[0.5(1+\exp(-TR/T_1))]$, where T_1 is the longitudinal relaxation time of blood and TR refers to the duration of the RR interval.

Shortening both TE and inter-echo spacing may be of particular interest for cardiovascular applications where flow and motion artifact suppression is mandatory while a high SNR and short acquisition window are needed. In general, inter-echo spacing is governed by either 2TE or inter-180° gradients’ duration, whichever is longer. In practice, when maximum gradient strength and maximum slew-rates are utilized, TE becomes the limiting factor and the minimum echo time (TE) and inter-echo spacing are governed by the duration of the slice selection plus refocusing gradient (Go, Figure 1a).

To reduce the number of phase-encoding steps while maintaining the spatial resolution, inner-volume imaging was proposed using FSE with orthogonal 90° and 180° refocusing pulses (6) as shown in Figure 1a. However, using that approach, the signal from the

surrounding tissue will not be entirely avoided. If, however, the initial slice-selective 90° pulse was replaced by a 2D-selective cylindrical excitation perpendicular to the imaging plane (Figure 1b), the resultant signal will originate from a disc localized at the intersection between the 90° cylindrical and the slice selective 180° pulses (6). Such LocEx enables simultaneous small-FOV imaging in both phase-encode and read-out directions.

2D RF Pulse Design

The analytical approach from Pauly et al. (10) was adopted for the design of 2D-selective pulses with large flip angles and user-specified geometric constraints. 2D-selective excitation and inversion of magnetization require the simultaneous application of a radiofrequency (RF) waveform and amplitude-modulated gradient fields in two directions. Aiming at a cylindrical excitation profile, a spiral k-space trajectory (22) was performed using the gradient waveform $\mathbf{G}(t)$ parameterization proposed in (23). Balancing pulse duration against profile fidelity, the spiral k-space extension was chosen to cover the central lobe and the first negative and positive sidelobes of the jinc function. The latter represents the targeted cylindrical 2D pulse shape in k-space and determines the RF waveform $\mathbf{B_1}(t)$ (Figure 2). A numerical pulse simulation was implemented to assess the excitation pulse pattern. T2* decay during the excitation pulse was counteracted by pre-emphasizing early RF waveform samples, using T2* = 35ms (24,25).

Implementation on the scanner

The 2D-selective 90° cylindrical excitation using a spiral k-space trajectory was implemented as part of a DIR BB-FSE imaging sequence as shown in Figure 1 on a commercial 3T Philips Achieva MRI system equipped with a 62mT/m; 110mT/m/ms gradient system. Total pulse duration was 6ms with a <1% increase of SAR/maximum allowed SAR. To support a reduced specific absorption rate (SAR), the 180° refocusing pulse was followed by a train of 160° pulses. To suppress respiratory motion artifacts, a real-time prospective adaptive real-time navigator correction (26) was combined with the LocEx technique. Localization, angulations about all the three major axes, and the diameter of the cylindrical excitation are prescribed on the graphical user interface of the scanner console. Additional parameters of the pulse that can be defined by the user include the number of side-lobes (see Figure 2b) that are covered by $\mathbf{k}(t)$ in excitation k-space, and the distance of the first concentric aliasing ring from the central lobe in the image domain (Figure 2c). The former has an influence on the spatial selectivity of the 2D-selective pulse and the latter helps to avoid unwanted signal enhancement as a result of discretization in excitation k-space.

A 32-channel phased array cardiac receiver coil was used in all experiments. Sixteen anterior and 16 posterior coil elements were used simultaneously for signal reception.

Phantom Experiments

To interrogate the signal suppression characteristics of LocEx pulses, a cylindrical gel phantom was utilized (T_1/T_2=1200/100ms). Diameter and height of this cylinder was 20 cm. Phantom measurements were obtained using conventional 2D FSE imaging (TR=2s, slice thickness=8mm, RF excitation angle=90°, echo train length (ETL)=6, TE=12ms). Reference images, acquired without and with LocEx, had a FOV of 240mm and a matrix of 352×352 (Figure 3a,b). The same acquisition was then repeated using a reduced FOV (FOV=120mm, matrix of 176×176) *with* and *without* LocEx (LocEx diameter=100mm, Figure 3e,f). On the resultant images, signal intensity profiles in foldover direction were obtained (Figure 3g).

$watermark-text
$watermark-text
$watermark-text

$watermark-text

$watermark-text

$watermark-text

Normal Subject Experiments

Ten healthy adult subjects (age range: 24–45 years, 7 males) were examined in the supine position. All experiments were approved by the Institutional Review Board. Informed consent for scanning and participation was obtained from all participants. The study was Health Insurance Portability and Accountability Act compliant. Axial anatomic slices were planned at a mid-ventricular level of the heart during diastole. Data were acquired using navigator-gated and corrected (26) free-breathing dual-inversion 2D FSE imaging. The navigator was localized at the lung-liver interface of the right hemi-diaphragm, the gating window was 5mm, and a correction factor of 0.6 (27) was used. The "slice tracking" correction shifts the imaged slice position in the superior-inferior (SI) direction for each data segment acquisition. It has been shown that respiration-induced cardiac SI displacement amounts to 60% of that of the diaphragm (27). To characterize the utility of LocEx cardiac BB FSE imaging, five different datasets were collected at the same anatomical location in each subject. With these scans, we sought to investigate whether motion artifacts from stationary tissue can be reduced, whether the time efficiency of the data acquisition can be improved, and whether signal loss due T2* can be minimized. Dataset details are listed in Table 1. The first reference dataset, called RefFv, has a large FOV without LocEx (slice thickness=8mm, FOV=340×340mm, matrix = 352×352), an echo-train length (ETL) of 6, TR=2 cardiac cycles, and TE=12ms, which was the minimum TE possible under this protocol. The second reference dataset, called RefLx, has a large FOV as well but includes a user-defined 90° LocEx pulse with a diameter of 150 mm, a first order aliasing ring radius of 400 mm, and 2 side lobes covered in excitation k-space. The remaining datasets were all acquired with a reduced FOV (rFOV = 170×170 mm^2), unchanged LocEx configuration, and a matrix of 176×176, which is exactly half of that from RefFv. The third dataset (Lx) had TE remained unchanged. The fourth dataset (LxTE↓) had a shortened TE of 7ms. The fifth dataset (LxTE↓EL↑) had a short TE of 7ms, but the ETL was increased to 11 so that total acquisition window duration is identical to that of the reference scan. In all datasets, low-high k-space ordering with 62.5% partial coverage in fold-over direction was employed.

Normal Subject Data Analysis

Image processing and statistical analyses were performed off-line on a personal computer using an in-house custom-built software tool developed using Matlab® ver. 7.6 (Mathworks, Natick, MA). Two sets of quantitative measurements were performed. The first group of measurements was performed for all the images obtained with the different settings listed in Table 1. Myocardium SNR and myocardium-blood contrast-to-noise ratio (CNR) were calculated using the formulas SNR=S_{heart}/σ_{lung} and CNR=$(S_{heart}-S_{blood})/\sigma_{lung}$, respectively. Mean signal intensities S_{heart} and S_{blood} were calculated on two manually selected circular regions of interest (ROI) with a diameter of 10 mm in the center of the free wall of left ventricular myocardium and left ventricular blood pool, respectively. For consistent noise measurements and due to the lack of adequate regions for measurement of noise in the background in all small FOV scans, noise standard deviation σ_{lung} was calculated in a manually selected ROI (diameter=25mm) in the lungs where no anatomical structures could be visually identified. The edge sharpness of the left-ventricular lateral epicardium was also measured objectively similar to that described in (28). Briefly, the edge was traced manually by drawing points along the edge. Direction of maximum intensity variation was identified automatically perpendicular to the interface before a 1D Gaussian shape was modeled along the direction of maximum intensity variation at each point. Edge-sharpness was then calculated as the slope of the Gaussian shape.

The second set of measurements were performed on the RefFv and RefLx datasets to assess the effectiveness of signal suppression and the amount of residual structural artifacts in suppressed areas after using the 2D selective pulses. Air $SNR_{air}=m_{air}$ (air signal mean)/σ_{air}

$watermark-text

$watermark-text

$watermark-text

(air noise standard deviation) was calculated from RefLx in a region outside of the body posterior to the left shoulder. Mean signal intensity $S_{shoulder}$ was calculated in the posterior lateral upper back muscle. $SNR_{ha}=S_{heart}/\sigma_{air}$ and $SNR_{sa}=S_{shoulder}/\sigma_{air}$ were then calculated for RefFv and RefLx and the thus obtained results were compared.

Nonparametric analysis of variance (ANOVA) using Friedman analysis was performed on the SNR, CNR, and sharpness to assess whether these measurements from the eight methods in Table 1 were significantly different. This was followed by paired Wilcoxon's signed-rank analyses between the methods. In all multiple comparison analyses, Bonferroni correction was employed and a p-value ≤ 0.05 was considered statistically significant. MedCalc® version 11.6 (MedCalc Software, Mariakerke, Belgium) was used for statistical analysis.

RESULTS

Simulation and Phantom Measurements

The Bloch equation (8,10) simulation results for the 2D-selective pulse are visualized in Figure 2. The most prominent geometrical features of the 2D-selective pulses include the central-lobe, representing the target excitation and the (unwanted) concentric aliasing-ring related to k-space discretization (Figure 2c). Moreover, the aliasing-free region between the central lobe and the aliasing ring is clearly visible. Aliasing-free imaging is possible if the central lobe is localized inside the imaged FOV while the aliasing ring is outside of the object that is imaged.

Figure 3 demonstrates local exciation imaging in a phantom. The full FOV without and with LocEx are shown in Figure 3a,b, respectively. As predicted, images with reduced FOV with LocEx (Figure 3e) were void of any fold-over artifacts while without LocEx, severe fold-over distortion occured (Figure 3f, g, dashed arrows). In agreement with the numerical simulations displayed in Figure 2, signal intensity profiles obtained from the reduced FOV LocEx images (Figure 3g) as well as the noise floor images (Figure 3c,d) show substantial suppression of structures from outside the area of the local excitation compared to those without LocEx (solid arrows).

Normal Subject Measurements

Scans were completed successfully in all subjects. Table 1 summarizes the scan time for a single slice and the quantitative findings (SNR, CNR, and edge sharpness) from the *in vivo* study. A representative set of example images obtained in one of the study subjects is displayed in Figure 4.

SNR and CNR—Comparing the two full FOV examples RefFv and RefLx, the plain utilization of local excitation in RefLx resulted in a statistically significant improvement in SNR (87 vs. 71, p<.05) and CNR (82 vs. 66, p<.05), where noise was measured in the lung region and structural artifacts were considered. However, the change in SNR_{ha} from RefFv to RefLx was not significant (78±31 vs. 86±29, p=NS). This improvement is consistent with the expectation that respiratory motion induced artifacts are reduced with local excitation as clearly demonstrated in Figure 4 ((a) RefFv versus (b) RefLx, dashed arrows). When local excitation was further used in conjunction with a 50% reduction of the FOV, (Figure 4, Lx scans vs. Ref scans), no foldover artifacts were observed in the small-FOV images despite the fact that the FOV was substantially smaller than the cross section of the thorax.

Reduced FOV combined with a reduced number of phase encoding steps (Lx1) (while maintaining spatial resolution) led to both a reduced SNR (55 vs. 71; p<.05) and CNR (51 vs. 66; p<.05) when compared to RefLx. This is consistent with the associated reduction in

$watermark-text

$watermark-text

$watermark-text

scanning time. Remarkably, and despite the 2-fold reduction in scanning time, SNR and CNR values of all reduced FOV techniques had SNR and CNR that are slightly reduced when compared to those of RefFv (p=NS). However, SNR and CNR of all these scans were significantly low when compared to RefLx ($p<0.05$).

Edge Sharpness—As shown in Table 1, the use of local excitation techniques invariably was associated with improved edge sharpness in comparison to RefFv ($p<.05$).

Effect of TE and ETL—Complementary to imaging time and motion artifact reduction, the self-refocusing property of the 2D-selective LocEx was further exploited to shorten TE in FSE imaging. In our protocol, the self-refocused pulse enabled the reduction of the minimum TE from 12ms to 7ms with a resultant shortening of both inter-echo spacing (from 24ms to 14ms) and temporal resolution (from 72ms to 42ms), as demonstrated in the datasets from LxTE↓ and Lx (Figure 4). When comparing Lx vs. LxTE↓, improved visual edge definition (Figure 4, solid arrows) was consistent with the numerical findings related to sharpness (48 vs. 40, $p<.05$). It is noteworthy that the gain in edge sharpness associated with short TE was partly lost when ETL increased (p=NS). Moreover, using shorter TE helped to compensate in part for the SNR and CNR loss associated with rFOV. Shorter TE also improved SNR (61 vs. 55) and CNR (56 vs. 51) in LxTE↓ when compared to its long TE counterpart Lx. However, this was not statistically significant. Scan LxTE↓TL↑ (Figure 4) further demonstrates that the shortened TE and inter-echo spacing can be used to reduce the total scan time by 70%.

Residual Artifacts—The left panel of Figure 4 displays zoomed and leveled views of an outer volume region before and after suppression. Successful signal suppression can be appreciated using local excitation. Statistically, SNR_{sa} in RefFv was effectively suppressed when compared to that of RefFv (3.8±1.0 vs. 46.4±23, $p<.05$). In the RefLx datasets, SNR_{sa} was slightly higher than SNR_{air} (3.8±1.0 vs. 3.1±0.8, $p<.05$).

DISCUSSION

In DIR cardiovascular imaging, motion artifacts originating from the chest wall, motion during the signal-readout, and relative motion induced by slice tracking adversely affect image quality. Therefore, there is a strong need for techniques that enable local excitation and reduced FOV imaging in cardiovascular MRI. To address that, a new free-breathing DIR 2D local excitation inner-volume technique has been developed and implemented to test the following hypotheses: (1) significant scan reduction can be obtained by using local excitation and reduced FOV imaging; (2) LocEx helps reduce artifacts originating from outside the area of interest; (3) LocEx in combination with rFOV adds flexibility in the choice of imaging parameters, which can be exploited to improve SNR, CNR, and temporal resolution.

With local excitation in black-blood cardiac FSE imaging, it became possible to reduce both FOV and scan time by 50%. As demonstrated above, local excitation of the heart and suppression of the chest wall and other surrounding static structures may lead to a reduced motion artifact level and improved SNR, CNR, and image clarity. For imaging approaches which include prospective adaptation of the imaged volume position (29) or self-navigation techniques with retrospective correction, this might be of particular interest. In these applications, the imaged volume position is adapted to match that of the anatomy of interest. However, this leads to an apparent displacement of the otherwise static background tissue and to resultant motion artifacts. These can be significantly avoided with inner-volume techniques and is in line with the present findings. As a result, local excitation may be particularly well-suited for coronary MRA and coronary vessel wall imaging that includes

$watermark-text

$watermark-text

$watermark-text

prospective or retrospective adaptation of the imaged volume position (29). In BB-FSE imaging of the heart, motion-related artifacts often adversely affect image quality. While motion artifacts may also be reduced using orthogonal-slab inner-volume imaging (6), TE can be additionally shortened when using self-refocused 2D-selective pulses which leads to a further reduction of such motion artifacts. A shortened TE leads to a reduction of T2*-related artifacts and T2-weighted k-space modulation. This affords the advantage of an increased signal and reduced inter-echo spacing and can be exploited to improve the temporal resolution (shorter acquisition window). Since motion artifacts are amplified with prolonged TE, the local excitation technique with shortened TE is expected to be advantageous for high heart rates. Shortened TE can also be utilized to accelerate the scan since more profiles in k-space can be acquired per unit time (if the duration of the acquisition window remains unchanged).

Gaussian-distribution magnitude noise measurements in the air (30) were not feasible on reduced FOV images. Alternatively and since the same receiving coil was used in all measurements, modulus magnitude Rician and Raleigh distributed noise was calculated from regions with a minimal amount of anatomical structures and the relative SNR and CNR measurements were calculated. While respiratory motion and flow artifacts are not part of the random image noise, they appear as spurious signal that affects noise statistics and therefore the actual in vivo cardiac SNR and CNR measurements.

Local excitation was combined with a standard FSE sequence available on the scanner. The refocusing pulses plus crusher gradients around these were not modified as a result of our implementation and the crusher's 1st moment was 5.9mT.ms^2/m in all scans. Therefore, it is expected that any FSE crusher or refocusing optimization may equally benefit the original and the modified FSE sequences utilized in this study.

Since the early introduction of 2D local excitation to MR spectroscopy (9), various local excitation techniques have been developed but have not been exploited for high spatial resolution motion-suppressed high-field cardiac imaging. 2D-selective pulses have already successfully been exploited as pre-pulses for spin labeling coronary MR angiography (31) or "local dual-inversion" for coronary vessel wall imaging (32). While the inner volume technique (6) successfully demonstrated reduced FOV imaging of the heart, to our knowledge, this is the first study that demonstrates the feasibility and the potential benefits of the direct integration of a 2D-selective pulse into the imaging part of free-breathing navigator-gated and corrected dual-inversion black-blood FSE cardiac imaging at 3T.

The current LocEx inner-volume imaging technique may not be suited for multislice 2D imaging (33) without modifications. However, in cardiac imaging, the acquisition window has to be small and is often constrained to the diastolic, most quiescent period of the cardiac cycle while the temporal resolution has to be high to avoid motion blurring and artifacts. Therefore, there is limited opportunity for such multislice 2D black-blood imaging of the heart in general and the limitation for multislice LocEx inner-volume black-blood imaging seems relatively minor. Particularly, and for improved volumetric coverage, the combination of the local excitation technique with segmented k-space 3D signal readout seems straightforward but remains to be investigated.

Although 3D inner-volume imaging of the heart was originally reported as a means to obtain full 3D coverage, the focus here was on 2D imaging for a comprehensive validation. However, the sequence can be extended to 3D imaging and improved time efficiency with improved volumetric coverage is expected. As an example, for 3D imaging, a 50% reduced FOV and a 50% reduced matrix will result in an SNR penalty of $1/\sqrt{2}$ while scan time is reduced by 50%. However, twice as many slices with doubled volumetric coverage could be

$watermark-text

$watermark-text

$watermark-text

acquired which, in theory, compensates for the 1/√2 SNR penalty while scanning time remains unchanged. An additional gain in scan time or volumetric coverage may be obtained if the shortened TE was also utilized to acquire more k-space profiles during the acquisition window.

In addition to the potential for accelerated 3D FSE imaging, other imaging sequences may be among the beneficiaries of 2D-selective self-refocused pulses at high magnetic field strength. Local excitation can theoretically be integrated into Echo Planar Imaging (EPI), GRASE(34), and MSDE (35). However, the duration of such 2D-selective pulses is currently in the order of 5–10ms and therefore they may not be well-suited as part of segmented k-space gradient echo imaging sequences or steady-state with free precession approaches. However, with advances in scanner hardware and particularly multitransmit capabilities (24,36), such 2D-selective pulses may be abbreviated significantly, which may enable the use of 2D-selective pulses as part of segmented k-space gradient echo imaging sequences as well.

CONCLUSION

Local excitation was implemented for *in vivo* free-breathing navigator gated and corrected inner-volume black-blood cardiac imaging at 3T by combining a 2D-selective RF excitation pulse with an FSE signal-readout at 3T. As a result, signal is exclusively obtained from the heart while that of the surrounding structures is effectively suppressed. Therefore, black-blood small-FOV imaging of a user-specified region in the human thorax is feasible, motion artifacts are minimized, time efficiency is improved and additional flexibility in the choice of imaging parameters supports both shorter scan times and reduced acquisition window duration.

Acknowledgments

Grant Support: This work was supported by the NIH/NHLBI research grant RO1HL084186

This work is supported by a grant R01-HL084186 from the National Heart, Lung, and Blood Institute.

References

1. Crowe LA, Gatehouse P, Yang GZ, Mohiaddin RH, Varghese A, Charrier C, Keegan J, Firmin DN. Volume-selective 3D turbo spin echo imaging for vascular wall imaging and distensibility measurement. J Magn Reson Imaging. 2003; 17(5):572–580. [PubMed: 12720267]
2. Saekho S, Boada FE, Noll DC, Stenger VA. Small tip angle three-dimensional tailored radiofrequency slab-select pulse for reduced B1 inhomogeneity at 3 T. Magn Reson Med. 2005; 53(2):479–484. [PubMed: 15678525]
3. Wilm BJ, Svensson J, Henning A, Pruessmann KP, Boesiger P, Kollias SS. Reduced field-of-view MRI using outer volume suppression for spinal cord diffusion imaging. Magn Reson Med. 2007; 57(3):625–630. [PubMed: 17326167]
4. Greenman RL, Shirosky JE, Mulkern RV, Rofsky NM. Double inversion black-blood fast spin-echo imaging of the human heart: a comparison between 1.5T and 3. 0T. J Magn Reson Imaging. 2003; 17(6):648–655. [PubMed: 12766893]
5. Lee VS, Hecht EM, Taouli B, Chen Q, Prince K, Oesingmann N. Body and cardiovascular MR imaging at 3. 0 T. Radiology. 2007; 244(3):692–705. [PubMed: 17709825]
6. Feinberg DA, Hoenninger JC, Crooks LE, Kaufman L, Watts JC, Arakawa M. Inner volume MR imaging: technical concepts and their application. Radiology. 1985; 156(3):743–747. [PubMed: 4023236]
7. Bottomley PA, Hardy CJ. Two-dimensional spatially selective spin inversion and spin-echo refocusing with a single nuclear magnetic resonance pulse. J Appl Phys. 1987; 62(10):4284–4290.

$watermark-text

$watermark-text

$watermark-text

8. Pauly JM, Nishimura DG, Macovski A. A k-space analysis of small-tip-angle excitation. J Magn Reson. 1989; 81:43–56.
9. Bottomley PA. Spatial localization in NMR spectroscopy in vivo. Ann N Y Acad Sci. 1987; 508:333–348. [PubMed: 3326459]
10. Pauly JM, Nishimura DG, Macovski A. A linear class of large-tip-angle selective excitation pulses. J Magn Reson. 1989; 82:571–587.
11. Mitsouras D, Mulkern RV, Afacan O, Brooks DH, Rybicki FJ. Basis function cross-correlations for robust k-space sample density compensation, with application to the design of radiofrequency excitations. Magn Reson Med. 2007; 57(2):338–352. [PubMed: 17260377]
12. Xu D, King KF, Zhu Y, McKinnon GC, Liang ZP. A noniterative method to design large-tip-angle multidimensional spatially-selective radio frequency pulses for parallel transmission. Magn Reson Med. 2007; 58(2):326–334. [PubMed: 17654576]
13. Saekho S, Yip CY, Noll DC, Boada FE, Stenger VA. Fast-kz three-dimensional tailored radiofrequency pulse for reduced B1 inhomogeneity. Magn Reson Med. 2006; 55(4):719–724. [PubMed: 16526012]
14. Mitsouras D, Mulkern RV, Rybicki FJ. Strategies for inner volume 3D fast spin echo magnetic resonance imaging using nonselective refocusing radio frequency pulses. Med Phys. 2006; 33(1): 173–186. [PubMed: 16485424]
15. Yip CY, Fessler JA, Noll DC. Iterative RF pulse design for multidimensional, small-tip-angle selective excitation. Magn Reson Med. 2005; 54(4):908–917. [PubMed: 16155881]
16. Davies NP, Jezzard P. Selective arterial spin labeling (SASL): perfusion territory mapping of selected feeding arteries tagged using two-dimensional radiofrequency pulses. Magn Reson Med. 2003; 49(6):1133–1142. [PubMed: 12768592]
17. Crowe LA, Keegan J, Gatehouse PD, Mohiaddin RH, Varghese A, Symmonds K, Cannell TM, Yang GZ, Firmin DN. 3D volume-selective turbo spin echo for carotid artery wall imaging with navigator detection of swallowing. J Magn Reson Imaging. 2005; 22(4):583–588. [PubMed: 16161101]
18. Bornstedt A, Bernhardt P, Hombach V, Kamenz J, Spiess J, Subgang A, Rasche V. Local excitation black blood imaging at 3T: application to the carotid artery wall. Magn Reson Med. 2008; 59(5):1207–1211. [PubMed: 18421686]
19. Edelman RR, Chien D, Kim D. Fast selective black blood MR imaging. Radiology. 1991; 181(3): 655–660. [PubMed: 1947077]
20. Simonetti OP, Finn JP, White RD, Laub G, Henry DA. “Black blood” T2-weighted inversion-recovery MR imaging of the heart. Radiology. 1996; 199(1):49–57. [PubMed: 8633172]
21. Fleckenstein JL, Archer BT, Barker BA, Vaughan JT, Parkey RW, Peshock RM. Fast short-tau inversion-recovery MR imaging. Radiology. 1991; 179(2):499–504. [PubMed: 2014300]
22. Crelier, GR. Two-Dimensionally Selective Excitation for Cardiovascular Magnetic Resonance Imaging. Zürich: ETH Swiss Federal Institute of Technology; 1996. p. 93
23. Bracewell, RN. The Fourier transform and its applications. Vol. xx. Boston: McGraw Hill; 2000. p. 616
24. Lee D, Lustig M, Grissom WA, Pauly JM. Time-optimal design for multidimensional and parallel transmit variable-rate selective excitation. Magn Reson Med. 2009; 61(6):1471–1479. [PubMed: 19365849]
25. Storey P, Thompson AA, Carqueville CL, Wood JC, de Freitas RA, Rigsby CK. R2* imaging of transfusional iron burden at 3T and comparison with 1. 5T. J Magn Reson Imaging. 2007; 25(3): 540–547. [PubMed: 17326089]
26. Danias PG, McConnell MV, Khasgiwala VC, Chuang ML, Edelman RR, Manning WJ. Prospective navigator correction of image position for coronary MR angiography. Radiology. 1997; 203(3):733–736. [PubMed: 9169696]
27. Wang Y, Ehman RL. Retrospective adaptive motion correction for navigator-gated 3D coronary MR angiography. J Magn Reson Imaging. 2000; 11(2):208–214. [PubMed: 10713956]
28. Botnar RM, Stuber M, Danias PG, Kissinger KV, Manning WJ. Improved coronary artery definition with T2-weighted, free-breathing, three-dimensional coronary MRA. Circulation. 1999; 99(24):3139–3148. [PubMed: 10377077]

$watermark-text

$watermark-text

$watermark-text

29. McConnell MV, Khasgiwala VC, Savord BJ, Chen MH, Chuang ML, Edelman RR, Manning WJ. Prospective adaptive navigator correction for breath-hold MR coronary angiography. Magn Reson Med. 1997; 37(1):148–152. [PubMed: 8978644]

30. Constantinides CD, Atalar E, McVeigh ER. Signal-to-noise measurements in magnitude images from NMR phased arrays. Magn Reson Med. 1997; 38(5):852–857. [PubMed: 9358462]

31. Katoh M, Spuentrup E, Barmet C, Stuber M. Local re-inversion coronary MR angiography: arterial spin-labeling without the need for subtraction. J Magn Reson Imaging. 2008; 27(4):913–917. [PubMed: 18383252]

32. Botnar RM, Kim WY, Bornert P, Stuber M, Spuentrup E, Manning WJ. 3D coronary vessel wall imaging utilizing a local inversion technique with spiral image acquisition. Magn Reson Med. 2001; 46(5):848–854. [PubMed: 11675634]

33. Feinberg DA, Mills CM, Posin JP, Ortendahl DA, Hylton NM, Crooks LE, Watts JC, Kaufman L, Arakawa M, Hoenninger JC, et al. Multiple spin-echo magnetic resonance imaging. Radiology. 1985; 155(2):437–442. [PubMed: 3983396]

34. Oshio K, Feinberg DA. GRASE (Gradient- and spin-echo) imaging: a novel fast MRI technique. Magn Reson Med. 1991; 20(2):344–349. [PubMed: 1775061]

35. Wang J, Yarnykh VL, Hatsukami T, Chu B, Balu N, Yuan C. Improved suppression of plaque-mimicking artifacts in black-blood carotid atherosclerosis imaging using a multislice motion-sensitized driven-equilibrium (MSDE) turbo spin-echo (TSE) sequence. Magn Reson Med. 2007; 58(5):973–981. [PubMed: 17969103]

36. Katscher U, Lisinski J, Bornert P. RF encoding using a multielement parallel transmit system. Magn Reson Med. 2010; 63(6):1463–1470. [PubMed: 20512848]

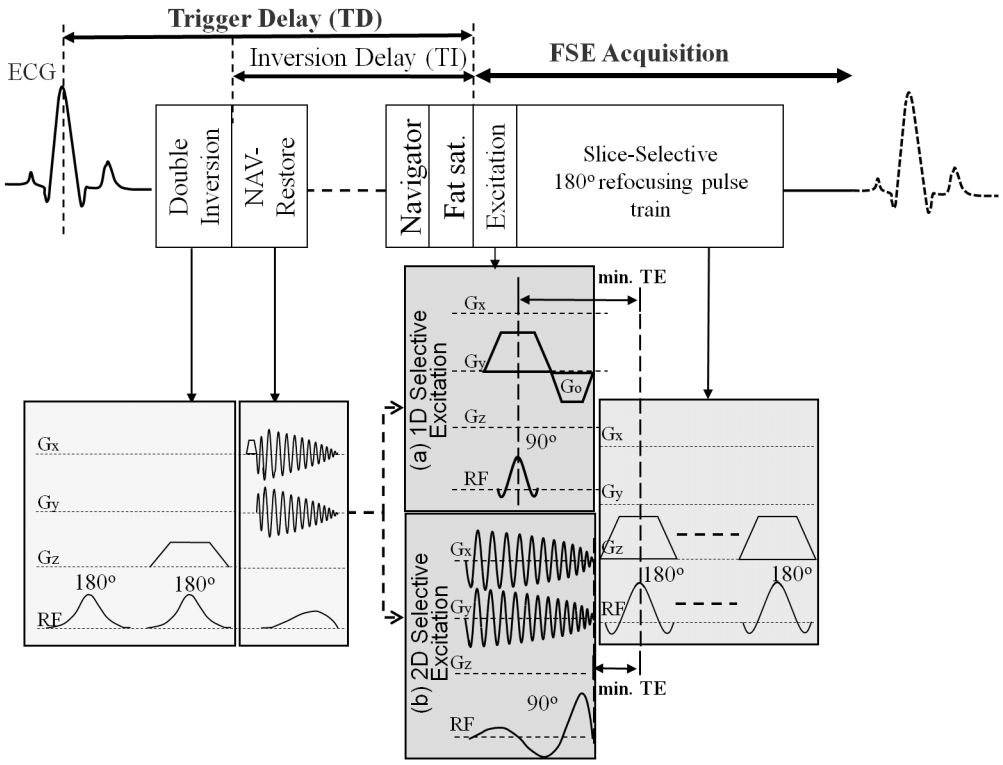

Figure 1.
Black-Blood FSE Sequence with motion-correction navigator and 2-D local excitation pulse with (a) 1D selective excitation in the phase-encoding direction and (b) 2D-selective excitation.

$watermark-text
$watermark-text
$watermark-text

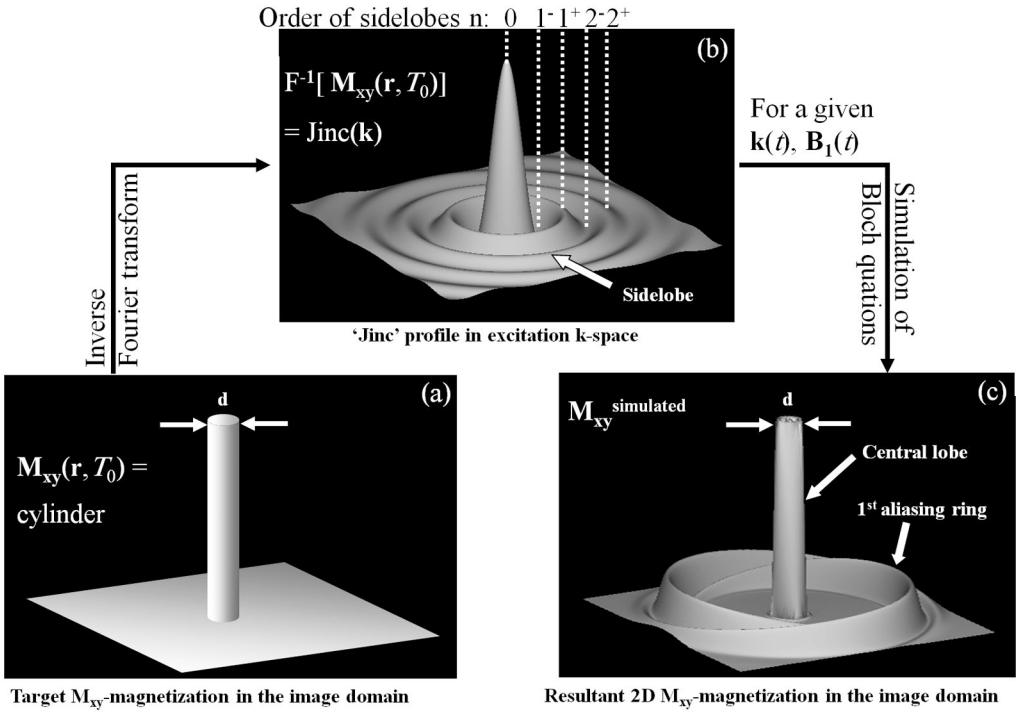

Figure 2.

The target $\mathbf{M_{xy}}$ magnetization in the image domain (a) corresponds to a 'jinc-function' in k-space (b). If $\mathbf{k}(t)$ is a spiral trajectory covering the central and the first two side lobes of the jinc, the simulation of the Bloch equation yields the final magnetization as shown in (c) where only M_{xy} is shown. The central lobe in (c) approximates the desired 2D excitation pattern (a), except for the aliasing ring, which is kept at distance by keeping adjacent spiral turns close enough.

$watermark-text
$watermark-text
$watermark-text

$watermark-text
$watermark-text
$watermark-text

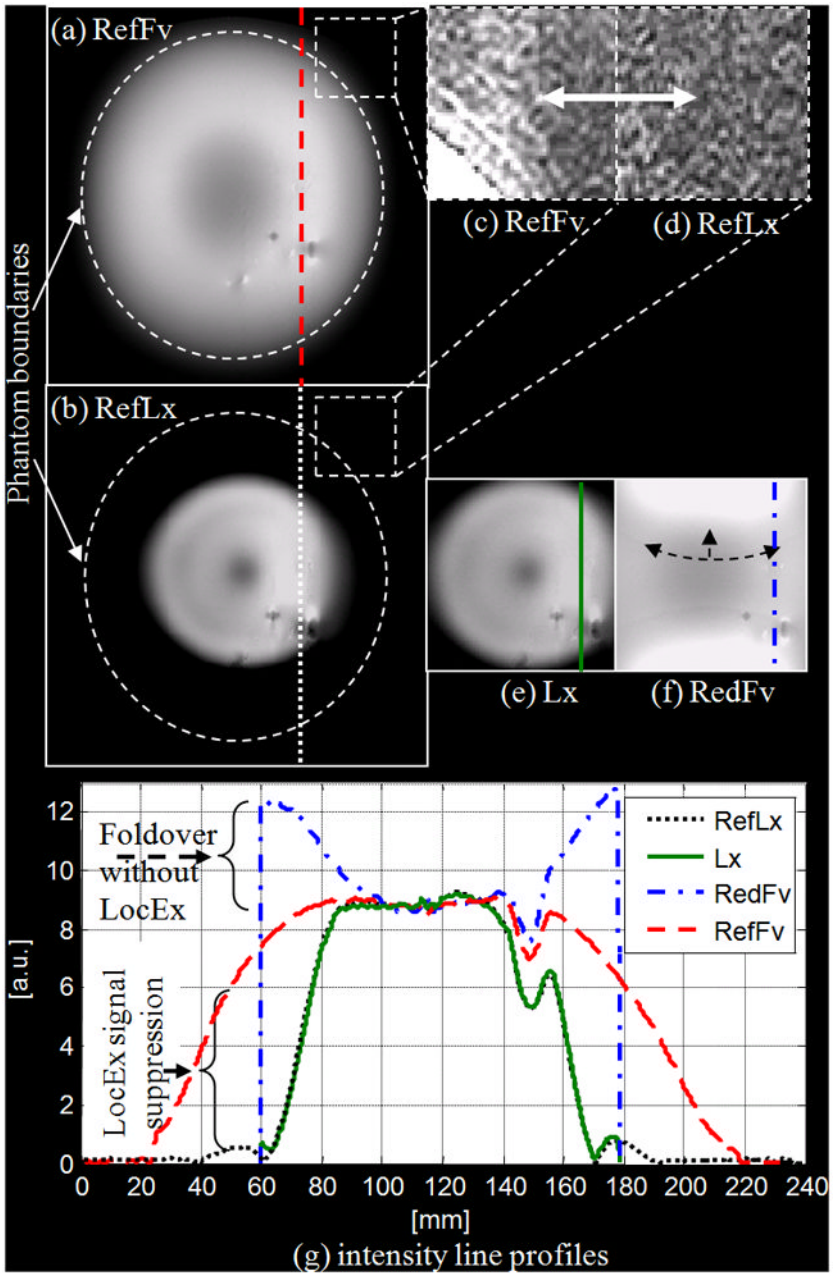

Figure 3.

Phantom images with (a) a large FOV without LocEx, (b) a large FOV with LocEx, (e) a small FOV with LocEx, and (f) a small FOV without LocEx. The noise floor is zoomed and leveled for better visualization of the effectiveness of the LocEx signal suppression (d) compared to RefFv (c). The intensity profiles at the level of the vertical lines in (a,b,e,f) are plotted in (g). Solid arrows in (c), (d), and (g) point to the extent of signal suppression as a result of LocEx. The dashed arrows in (f) and (g) point to the extent and amount of foldover artifacts in small FOV imaging, which was avoided when LocEx was utilized.

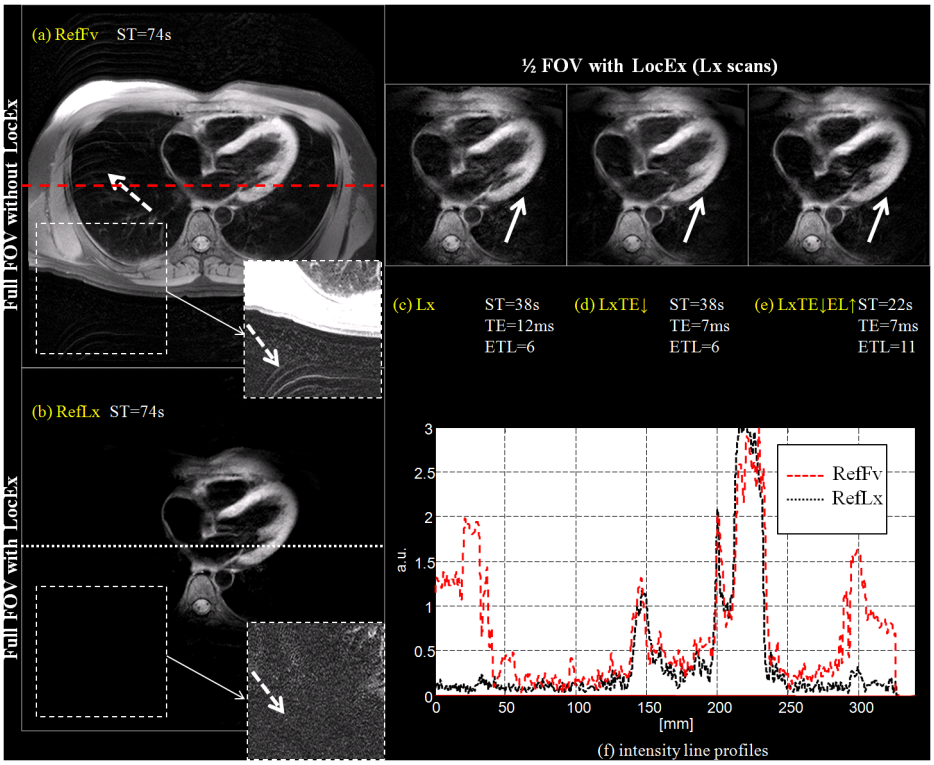

Figure 4.

Black-blood FSE Imaging using (a) full FOV (RefFv), (b) full FOV with LocEx (RefLx), and (c–e) various reduced FOV schemes (Lx, LxTE↓, and LxTE↓EL↑) demonstrating the potential use of 2D local excitation to reduce total scan time (ST) and/or to improve image quality. Dashed arrows point to reparatory motion induced artifacts that are suppressed by using local excitation. Although reduced FOV images had shorter scan duration, they were associated with sharper edge definition (solid arrows). (f) the signal intensity of a horizontal line through the heart using RefLx versus RefFv, demonstrating quantitatively the extent of signal suppression with LocEx utilization.

$watermark-text
$watermark-text
$watermark-text

$watermark-text $watermark-text $watermark-text

Table 1

MRI parameter settings and description. Independent parameters that have been changed are highlighted in gray.

	Dataset ID	b	TE (ms)	ETL	Acquisition window (ms)	Scan duration/ slice (heart cycles)	SNR	CNR	Edge Sharpness	Description and Hypothesis
A	**RefFv**	Full	12	6	72	74	***70.2±36.5*** †	***65.7±35.6*** †	***34.2±12.2*** †	***Reference dataset with full FOV without LocEx***
	RefLx	Full	12	6	72	74	91.4±43.8 *	85.9±43.1 *	42.2±11.3 *	Reference dataset with full FOV and local excitation (LocEx) to reduce motion and flow artifacts.
B	**Lx**	½FOV	12	6	72	38	55.3±14.6 †	50.8±13.3 †	40.2±13.6 *	Using LocEx with reduced FOV (rFOV) to reduce scan time by 50%.
C	**LxTE↓**	½FOV	7	6	42	38	60.8±24.9 †	56.1±23.3 †	47.6±15.3 *	To test the effect of a minimal possible TE on SNR and CNR (acquisition window, temporal resolution, and total scan time are reduced by %50).
D	**LxTE↓EL↑**	½FOV	7	11	77	22	56.5±15.8 †	52.2±15.6 †	44.7±17.2 *	To test the effect of a minimal possible TE and an increased ETL on SNR and CNR (acquisition window is unchanged, total scan time is reduced by %70).

*: p<.05, compared to RefFv.

†p<.05 compared to RefLx. (seven comparisons in each category)